Technology in Cancer Research & Treatment
ISSN 1533-0346
Volume 2, Number 6, December (2003)

Tissue Characterization by Quantitative Optical Imaging Methods

www.tcrt.org

Amir H. Gandjbakhche, Ph.D.[1,*]
Victor Chernomordik, Ph.D.[1]
David Hattery, Ph.D.[1]
Moinuddin Hassan, Ph.D.[1]
Israel Gannot, Ph.D.[1,2]

[1]Laboratory of Integrative and Medical Biophysics (LIMB)
National Institute of Child Health and Human Development (NICHD)
National Institutes of Health (NIH)
Bethesda, Maryland 20892 USA
[2]Department of Biomedical Engineering
Faculty of Engineering
Tel-Aviv University
Tel-Aviv 69978, Israel

Optical methods have a long history in the field of medical diagnosis. The biomolecular specificity possible with optical methods has been particularly valuable in microscopy and histopathology while *in vivo* imaging of deep structures has traditionally been the domain of X-ray and MRI. The use of optical methods in deep tissue has been limited by multiple-scattering which blurs or distorts the optical signal. New stochastic methods which account for multiple scattering have been developed that are extending the usefulness of optical methods deep into tissue. In optical mammography, photons may travel through 10cm of tissue before arriving at the detector. We have developed a method for quantifying parameters of anomalous sites in breast tissue that may be used for functional characterization of tumors. In other work presented here, we are developing fluorescence based methods to detect and monitor tumor status. The immune response to a tumor is a target for fluorescently labeled specific antibodies. We have developed a method to localize the tumor site using CW fluorescence. Additionally, we have developed a method which uses time-resolved data and capitalizes on probe lifetime sensitivity to metabolic parameters such as pH and temperature to obtain functional information from the tumor site.

Introduction

Optical imaging techniques have contributed to important discoveries in molecular and cell biology based on studies of single cells or *in vitro* tissue cultures. Use of lasers, high speed scanners, and modern electro-optical imaging devices have led to sophisticated technologies such as fluorescence microscopy, confocal microscopy, optical coherence tomography, and two-photon microscopy. However, these techniques are based on geometric optics of light rays passing through the objects of interest. Most tissues scatter light so strongly, however, that for geometric optics-based equipment to work, special techniques are needed to remove multiply scattered light (such as pinholes in confocal imaging or interferometry in optical coherence microscopies). Even with these special designs, high resolution optical imaging fails at depths of more than 500 microns below the tissue surface. As a result, *in vivo* optical imaging has traditionally been limited to superficial tissue surfaces directly or endoscopically accessible, and to tissues with a biological window (e.g., along the optical axis of the eye).

Visible or near infrared (NIR) light impinging upon most biological tissue is scattered many times in a distance of ~1mm. To analyze light-tissue interactions, one needs to take into account the diffusive nature of light propagation. In contrast to CT and Positron Emission Tomography (PET) which deal with ballistic photons, only statistical physics with a complex underlying theoretical picture can describe photon paths in order to separate the effects of scattering from absorption, and therefore provide reliable path-length estimation for noninvasive

* Corresponding Author:
Amir H. Gandjbakhche, Ph.D.
Email: amir@helix.nih.gov

spectral analysis of tissue changes, especially clinical assessment of physiological parameters and metabolic status. The main advantages of these techniques are to provide functional imaging modalities, in addition to density imaging, while avoiding ionizing radiation hazards.

For an optical imaging technique to be clinically useful, multi-disciplinary and multi-step approaches are required. One should devise quantitative theories, and develop methodologies applicable to *in vivo* quantitative tissue spectroscopy and tomographic imaging. At the bench, one designs and conducts experiments on tissue-like phantoms and runs computer simulations to validate the theoretical findings. The most difficult task is to bring the optical system from bench to bedside. Usually use of animal models, as an intermediate step, for pre-clinical studies is necessary. Strong collaborations among engineers, physicists and physicians are needed for identifying physiological sites where optical techniques may be clinically practical and can offer new diagnostic knowledge and/or less morbidity over existing methods.

Differentiation of structures and functional status *in vivo* relies on the ability of the imaging method to provide measurable optical contrasts. The most commonly used optical sources of contrast are endogenous or exogenous fluorescent labels, variations in absorption (e.g., hemoglobin or chromophore concentration) and scattering (tissue density and texture). The absorption coefficient, μ_a (mm^{-1}) represents the inverse mean pathlength of photon before absorption. In other words, $1/\mu_a$ is a distance in a medium where intensity is attenuated by a factor of 1/e (Beer's Lambert Law). Absorption in tissue is strongly wavelength dependent and is due to chromophores and water. Among the chromophores in tissue, responsible for its absorption properties, the dominant component in the visual range is the hemoglobin in blood. Below 650 nm it results in very strong tissue absorption. Another tissue component, important for light absorption, is the water. While water absorption is low in the visible and NIR region, it increases rapidly above approximately 950nm.

In high resolution optical methods and OCT where penetration is highly dependent on scattering, longer wavelengths with lower scattering coefficients may increase penetration. It should be taken into account, however, that these methods do not provide imaging capabilities below 1-2 mm in the case of highly scattering media, e.g., biological tissues. For greater penetration depth, multiple scattering is implicit and the depth of penetration will primarily depend on the absorption coefficient. Thus, for greatest penetration of light in tissue, wavelengths in the 650-1100 nm spectral range are typically used (1), so that absorption in this range is sensitive to concentrations of physiological (oxy- and deoxy-hemoglobin) and diagnostically importance. This region of the light spectrum is called "the therapeutic window". Similarly, scattering characterized by a coefficient, μ_s that is the inverse mean free path of photons between scattering events. Scattering in tissue is biased in the forward direction and is anisotropic, with parameter g being the coefficient of anisotropy. In tissues, g is typically *0.7* to *0.98* (2, 3). Likewise, different tissue types have differing scattering properties which are also wavelength dependent. The scattering coefficients of many soft tissues have been measured at a variety of optical wavelengths, and are within the range 10-100mm^{-1}. In comparison to absorption, however, scattering changes, as a function of wavelength, are more gradual and have smaller extremes.

Theories of photon migration are often based on isotropic scattering. Therefore, one must find the appropriate scaling relationships that will allow one to use an isotropic scattering model. For the case of diffusion like models (e.g., (4)), it has been shown that one may use an isotropic scattering model with a transport-corrected scattering coefficient, $\mu'_s = \mu_s (1\text{-}g)$.

There are instances in which the spectroscopic signatures will not be sufficient for detection of disease. This can occur when the specific disease results in only very small changes to the tissue's scattering and absorption properties, or when the scattering and absorption properties of the disease are not unique to the disease. In such cases, another source of optical contrast, such as fluorescence, will be required to detect and locate the disease. Presence of fluorescent molecules in tissues can provide useful contrast mechanisms. Concentration of these endogenous fluorophores in the body can be related to functional and metabolic activities, and therefore to the disease processes.

Advances in molecular biology of diseased processes, new immunohistopathological techniques, and the development of fluorescently-labeled cell surface markers have led to a revolution in specific molecular diagnosis of disease by histopathology, as well as in research on molecular origins of disease processes (e.g., using fluorescence microscopy in cell biology). As a result, an exceptional level of specificity is now possible due to the advances in the design of exogenous markers. Molecules can now be tailor-made to bind only to specific receptor sites in the body. These receptor sites may be antibodies or other biologically interesting molecules. Fluorophores may be bound to these engineered molecules and injected into the body, where they will preferentially concentrate at specific sites of interest (5, 6). The advent of nanoparticles has opened an exciting opportunity for such molecular imaging.

Furthermore, fluorescence may be used as a probe to measure environmental conditions in a particular locality by capitalizing on changes in fluorophore lifetimes (7, 8).

Among the projects underway in the Unit on Biomedical Stochastic Physics at NIH, we have chosen two projects to

be presented in this paper. The first one, ***Time-resolved Spectroscopy and Imaging of Human Breast***, deals with time-resolved imaging and spectroscopy of thick tissue and its application to quantification of functional parameters of breast tissue. The second project is the specific targeting of cells using fluorescence probes.

Time-resolved Spectroscopy and Imaging of Human Breast

Rationale

One of the most challenging areas to apply diffuse optical imaging of deep tissues is the human female breast (9-13). It is clear that any new imaging or spectroscopic modalities which can improve on diagnostics of breast tumors or can add new knowledge about the physiological properties of the tumors and surrounding tissues, will have significance in medicine. The potential scope of optical biopsy can be appreciated when it is realized that 186,000 cases of breast cancer are diagnosed each year in the USA, and aproximately 1 out of 10 all women in Western developed countries will experience a breast cancer during her life span. It has been shown that breast cancer mortality correlates with the metastatic status which again correlates with the size of the tumor (14, 15).

A great enthusiasm exists in the oncology community to test new therapies which include anti-angiogenic therapy, anti-vascular therapy, immunotherapy and gene therapy along with traditional therapy to improve the outcome. Monitoring tumor response that correlate to outcome is needed to properly evaluate neo-adjuvant therapy. Currently, there are no well-established non-invasive tests that can accurately predict tumors response to therapy. Our research goal is the evaluation of time–resolved optical imaging platform that may be able to supply this information.

As mentioned before, the fundamental problem with optical methods lies in the turbid nature of biological tissues that prevents embedded inclusions from being adequately resolved in optical images (16). This is the main reason for which conventional transillumination using continuous wave (*cw*) light, proposed several decades ago didn't achieve reasonable resolution (17, 18). In the late 1980's, time-resolved imaging techniques were proposed to enhance spatial resolution by detecting photons with very short time-of-flight within the tissue (19-23). In this technique a short laser pulse of ~ picosecond duration impinges upon the tissue. Transmitted photons experience dispersion in their pathlengths, resulting in temporal dispersion in their time-of-flight (TOF). The temporal and spatial information obtained from these TOF distributions can be used to extract information about optical properties of illuminated tissues (in particular, deeply embedded tissue abnormalities). Compared to the alternative frequency-domain mode of optical imaging, time-domain methods are expected to provide a richer informational content at the expense of some instrumental complexity (e.g., review (1)). However, recent technological advances in the field made these time-resolved techniques available not only for laboratory studies, but also for clinical optical mammography (13, 24, 25).

The goal of our group at NIH is to develop robust and efficient methods, based on the time-resolved spectral imaging, to quantify optical properties of the tissue abnormalities (e.g., tumors) as well as surrounding tissues at a given wavelength in the visible and/or near-infrared range, to investigate relationship between these optical properties, in particular, absorption coefficient, and composition of the tissue in question (i.e., oxy- and deoxy-hemoglobin concentration, water and lipid content), to analyze statistics of obtained physiological parameters (blood volume and oxygen saturation) of breast tissue and tumors in order to enhance specificity of diagnostics of tumors, detected by other imaging modalities or for treatment monitoring in clinical trials.

In *Theoretical Model and Phantom Experiments* we describe the validation of the theoretical model using experimental data, obtained from tissue-like phantoms, and Monte Carlo simulations. Substantiation of the model with "bench" experiments/simulations logically should be followed by the clinical *in vivo* measurements of tissue abnormalities (e.g., breast tumors) so-called "bedside" stage. We applied our theoretical algorithms to analyze such *in vivo* data. A description of the pilot results is presented in *Quantitative Spectroscopy of Breast Lesions*, where optical properties of tissue abnormalities (e.g., tumors) and surrounding background tissues at several wavelengths are estimated from actual *in vivo* time-resolved data, obtained from the first scanning optical mammograph, developed by our colleagues at PTB. In the last part we present our roadmap for future direction.

Theoretical Model and Phantom Experiments

Differing theoretical constructs have been proposed to analyze experimental data, using different photon time-of-flight or frequency intervals to separate the effects of scattering and absorption. This enables one to quantify optical coefficients as a spectroscopic signature of abnormal tissue embedded in thick, otherwise normal tissue. The most widely used of these theoretical constructs are the diffusion-like models based on the diffusion approximation of the transport equation and models based on random walk theory (RWT) (26).

Our group uses RWT on a cubic lattice, developed at NIH a decade ago, as a basis for theoretical analysis. Relationship between dimensionless RWT parameters (i.e., number of steps of the random walker n, its coordinates on the lattice r and N and absorption μ) and the corresponding physical

variables, necessary to analyze experimental data is well established (see, e.g., (27)):

$$n \to \mu_s^{(0)\prime} c\Delta t,\ r \to \overline{r}\ \frac{\mu_s^{(0)\prime}}{\sqrt{2}},\ \mu \to \frac{\mu_a^{(0)}}{\mu_s^{(0)\prime}}, \qquad [1]$$

where $\mu_s^{(0)\prime}$ is the transport-corrected background scattering coefficient $\mu_s^{(0)\prime} = \mu_s^{(0)}(1\text{-}g)$, $\mu_a^{(0)}$ is the background absorption coefficient, c is the speed of light in the medium (mm/ps), Δt is the photon time delay (28), $\overline{r}$ is the distance variable (9).

The optical contrast which can be calculated at each time delay is a relative perturbation in detected intensity $I(x, \Delta t)$, comparing to its background value $I(x_0, \Delta t)$, estimated from the measurements far from the abnormality in question:

$$C(x, \Delta t) = \frac{I(x, \Delta t) - I(x_0, \Delta t)}{I(x_0, \Delta t)} \qquad [2]$$

Theoretically time-dependent contrast functions are constructed from two quantities. First, the set of functions $\{P_n\}$ defined as the probability that a photon is detected at n^{th} step (i.e., time) in a homogeneous medium. Second, the set of functions (29) defined as the probability that a photon visits an abnormal site and then is detected at n^{th} step (i.e., time). $\{P_n\}$ correspond to intensities, while (29) correspond to point spread functions (PSF) for time-resolved imaging. Analytical expressions of these two quantities are given in papers (27, 30, 31).

To relate the contrast of the light intensity to the optical properties and location of abnormal targets in the tissue, we have taken advantage of some features of our theoretical framework. One is that the early time response is most dependent on scattering perturbations, whereas the late time behavior is most dependent on absorptive perturbations, thus allowing us to separate the influence of scattering and absorption perturbations on the observed image contrast. This is illustrated by Figure 1, where we present expected dependencies of the contrast components (32), as well as a total contrast on the photon time delay for optical parameters of the medium close to ones expected in tissues. It should be noted that scattering contrast is proportional in our model to the time-derivative of the PSF, dW_n/dn, divided by P_n, experimental data from Politechnico di Milano related to tissue-like phantom with abnormalities with increased scattering substantiate this prediction (see Fig. 2) (33).

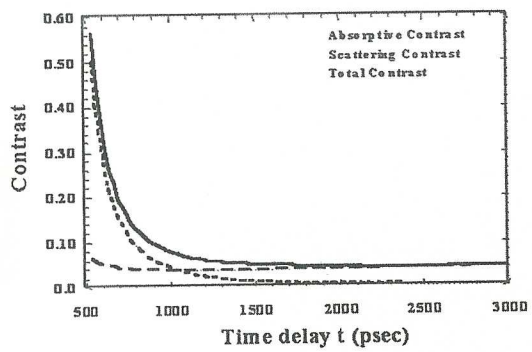

Figure 1: Behavior of absorbing (dotted curve) and scattering (dotted-dashed curve) contrasts and their sum (solid curve) as a function of time delay Δt.

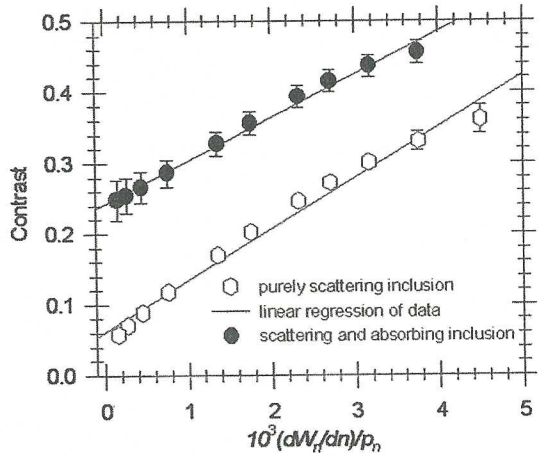

Figure 2: Linear dependence of contrast on the derivative of the PSF for inclusions with increased scattering and without increased absorption.

The second interesting feature in our methodology assumes that the contrast from scattering inside the inclusion is proportional to the cross-section of the target (in the z direction). This important feature of our theoretical construct was verified by analysis of an independent experimental data set obtained from researchers from *ART*, Quebec. Time-resolved contrast functions for three similar, purely scattering inclusions that differ only in size (d = 3.6, 5.0, 7.0 mm) were measured. In Figure 3, we present experimental contrast amplitudes as a function of the squared size of the inclusion for three values of time delay. In all cases the obtained dependence proved to be practically linear, passing through the origin, as we expect from our model.

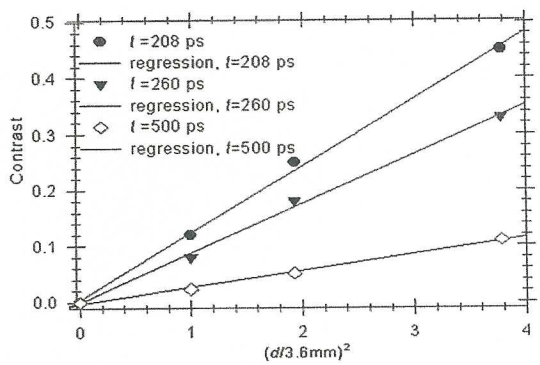

Figure 3: Dependence of contrast on the squared size of the scattering inclusion d^2 for different values of time delay.

We have derived a correction factor for large non-localized absorptive inclusions. This correction factor which takes into account effects of each absorptive unit (e.g., voxel) on

other units and vice versa. This correction factor has solved some discrepancies encountered in reconstructed images.

Unlike widely discussed in the literature diffusion optical tomography, our method poses less challenging (but hopefully easier achievable) goal. We do not try to reconstruct the whole 3-D distributions of optical parameters. Instead, our multi-step analysis of the collected data uses 2-D images observed at differing photon flight times to construct the time-dependent contrast functions, fit our theoretical expressions (forward model), and compute the optical properties of the background, and those of the abnormality along with its size. The outline of our data analysis is given in paper (34).

By utilizing our method for different wavelengths, one can obtain diagnostic information (for example, estimates of blood oxygenation of the tumor) for corresponding absorption coefficients that no other imaging modality can provide directly. Several research groups have already successfully used multi-wavelength measurements using frequency-domain techniques, to calculate physiological parameters (oxygenation, lipid, water) of breast tumors (diagnosed with other modalities) and normal tissue (e.g., 35-37).

We have verified our methodology, by applying it to a wide range of experimental data and Monte Carlo simulations made available to us by our colleagues from University College London (38): J. C. Hebden; from Politechnico di Milano (Italy): A. Pifferi, P. Taroni, A. Torricelli, G. Valentini, and R. Cubeddu; from Physikalisch-Technische Bundesanstalt and Robert-Roessle-Klinik, Charité, Humboldt University, (Germany): D. Grosenick, H. Wabnitz, H. Rinneberg, K. Thomas Moesta, and Peter M. Schlag; from Università degli Studi di Firenze (Italy): G. Zaccanti. An example of good agreement between reconstructed values of optical parameters and nominal ones for tissue-like phantoms from Politechnico di Milano is presented in Table I and II.

Table I
Estimated parameters for inclusion with increased absorption.

Parameters	Nominal Values	Reconstructed Values	Error (%)
μ_a (background)	0.01 mm^{-1}	0.0093 mm^{-1}	-7.0
μ_{sc}' (background)	1.0 mm^{-1}	1.06 mm^{-1}	6.0
μ_a (target)	0.04 mm^{-1}	0.038 mm^{-1}	-5.0
μ_{sc}' (target)	1.0 mm^{-1}	1.0 mm^{-1}	0.0
Size of the target	10.0 mm	12.2 mm	22.0

Table II
Estimated parameters for inclusion with increased scattering.

Parameters	Nominal Values	Reconstructed Values	Error (%)
μ_a (background)	0.01 mm^{-1}	0.0094 mm^{-1}	-6.0
μ_{sc}' (background)	1.0 mm^{-1}	1.06 mm^{-1}	6.0
μ_a (target)	0.01 mm^{-1}	0.0105 mm^{-1}	5.0
μ_{sc}' (target)	2.0 mm^{-1}	2.50 mm^{-1}	25.0
Size of the target	10.0 mm	9.7 mm	-3.0

Quantitative Spectroscopy of Breast Lesions

Verification of our RWT methodology of quantification of optical properties of abnormalities on the various tissue-like phantoms along with substantiation of the forward model with Monte Carlo simulations encouraged our transition from bench to clinical data, obtained *in vivo* from transillumination of human breast.

Pioneering work of Physikalich-Techniche-Bundesanstalt of Berlin (PTB) that has developed a first scanning time-domain optical mammograph provided a starting point for data analysis aimed at deriving useful information about breast lesions, in order to characterize their physiological properties.

The original version of the system uses an experimental set-up (Fig. 4), where the breast is slightly compressed between two glass plates (slab geometry). Short laser pulses at two wavelengths consecutively illuminate the breast. Source-detector pair is being moved in tandem over the opposite sides of the breast. The scanning approach has the advantage to directly yield raw projection images, without the need to apply sophisticated reconstruction procedures. 2-D

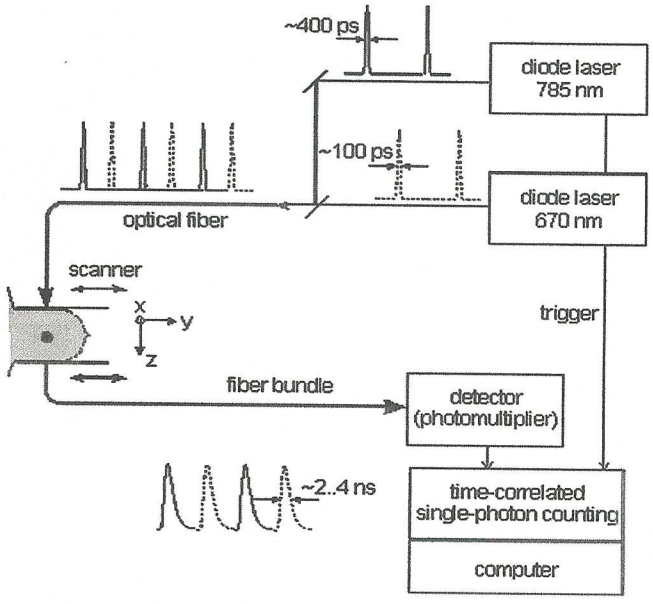

Figure 4: Block diagram of the laser pulse mammography.

optical mammograms can be generated from any specific quantity that can be derived from measured time-resolved transmittance data for each pixel. A scan of the whole breast takes but a few minutes, and can be done in mediolateral and craniocaudal geometries.

The most straightforward imaging method displays photon counts in selected time windows. It is useful to apply time windows that are adapted to the particular breast thickness and scattering which essentially determine the time scale for the distribution of times of flight (39).

In the frameworks of collaboration between NIH and PTB we have started investigation of *in vivo* clinical data, involving tumors embedded inside normal tissues. Our first goal is to quantify the optical parameters at several wavelengths and thereby estimate total blood volume and blood oxygen saturation of the tumor and surrounding tissue under the usual assumption that the chromophores contributing to absorption are oxy- and deoxy-hemoglobin, and water (40). Assessment of the *in vivo* data, as expected, proved to be more challenging than for the phantom data. Along with the intrinsic complications, such as inhomogeneity of the normal and malignant breast tissue, "edge effects" (not considered here) due to the decreasing thickness of compressed breasts close to their edges, and limited signal/noise ratio as well as the finite width

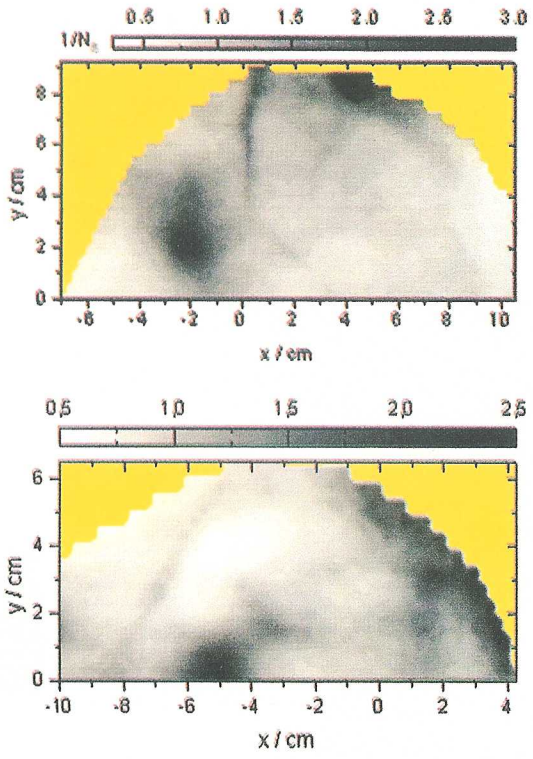

Figure 5: Optical mammograms of two patients with invasive ductal carcinomas, the mammograms display normalized inverse photon counts based on the late time window. **(a)** patient #9, craniocaudal view. **(b)** patient #11, mediolateral view.

of the instrument response function of the clinical device have to be taken into account. However, preliminary results are encouraging. We analyzed data sets, obtained at two wavelengths (670, 785nm), for four patients with invasive ductal carcinoma. The tumor can be easily seen in the corresponding optical images, corresponding to these patients (see, for example, Fig. 5a, b). In this figures, the image is obtained from reciprocal values of the total integrals of the distributions of times of flight of photons, normalized to a selected "bulk" area.

The background optical properties of breast tissue and the time-zero offset were estimated by averaging optical coefficients, found from curve fitting of time-resolved intensity distributions (see, e.g., Fig. 6), over more than 100 source-detector positions, taking into account the effect of instrumental response function.

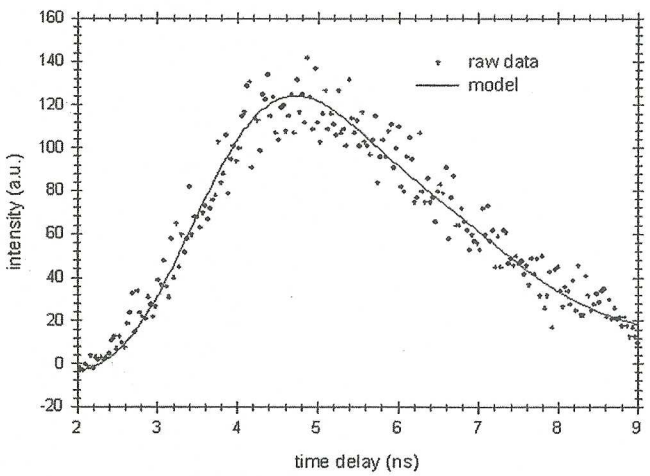

Figure 6: Data processing of typical time-resolved intensity distributions (deconvolution, filtering and curve fitting).

In the next step, a 2D set of time-resolved contrast functions was constructed, using measured intensity distributions corrected as described above. The maximum contrast spot was assumed to be the center of the abnormality. The shorter time delays provided a slightly better spatial resolution. Two linear contrasts scans, both passing through the center of abnormality, were calculated for different time delays. Curve fitting of these functions with the theoretical formula for absorptive contrast has been used to smooth the curves, calculate the absorptive component of the contrast and estimate the lateral size of the inclusion. Results of such curve fitting are illustrated by Figure 7 that presents the linear scans in *X*-direction for two time delays in the case of one of the patients.

The serious drawback of the current realization of the optical mammograph is that it does not provide a unique estimate of the abnormality depth. Independent scans with different relative source-detector positions, involving oblique angle source-detector geometry, are needed to overcome this

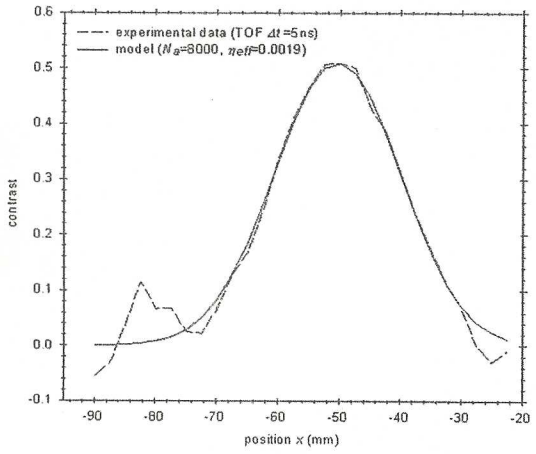

Figure 7: Example of a contrast scan along x-axis through tumor center (time of flight Δt=5 ns (patient #11).

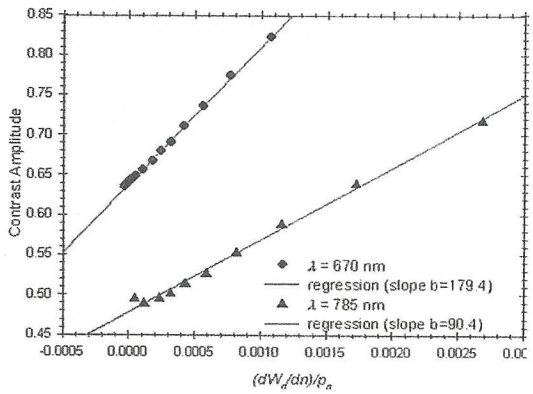

Figure 8: Dependence of tumor contrast (patient #9) on derivative of PSF for l = 670, 785 nm.

limitation. Some preliminary experimental results show that these additional scans do provide information on the abnormality's depth. They are to be incorporated into the future modifications of the mammograph. At the current stage to estimate optical parameters and sizes of the inclusion from the available data, an additional assumption about the depth of the abnormality must be made. For example, for one of the patients tumor depth was estimated from the histology findings, in another case, judging from the additional line scans with lateral offsets between the source and detector; it has been assumed that the tumor is close to the lower surface of the breast at the depth of $\overline{z}$ ~53 mm. In both of these cases using the assumed values of $\overline{z}$ results in reasonable estimates of the tumor optical parameters (see below).

As an example, below we briefly discuss the preliminary results of our analysis for the first two investigated cases (#9, 11 in the sampling list, see Tables III and IV). It was found that for both patients at both available wavelengths the contrast amplitude is decreasing with increasing time delay, indicating that considered tumors show increased scattering compared to surrounding tissue. To estimate the time delay $\Delta\tau$ inside abnormality, $\Delta\tau$ and the corresponding scattering perturbation $\Delta\mu_s'$ we determined the dependency of the contrast amplitude on the time derivative of the PSF. For the calculation of these derivatives the time-zero offset was used as obtained from the analysis of background optical properties as described above. This correction does not change noticeably the results for the tumor absorption coefficient which is determined by the contrast functions for relatively large time delays. Scattering perturbations, which are determined from the short time delays data, are expected to be sensitive to the choice of time-zero, as found to be the case.

In all cases considered the relationship between contrast amplitude and the PSF derivative proved to be close to linear for $\Delta t < \Delta t_{max}$, as expected in the theoretical model. This is illustrated in Figure 8, obtained from the data for one of the patients (#9 in the sampling list), where the relationship between the contrast amplitude and the PSF derivative is presented for λ = 670, 785 nm. The smaller slope for the infrared data, compared to the red data, implies a lower scattering perturbation at the longer wavelength. The calculated average slopes of the dependence of the contrast amplitude on the PSF derivative, in combination with estimated or assumed dimensions of the tumor, are used to evaluate the scattering perturbation, due to the tumor.

Comparison of the time-resolved contrast amplitudes for relatively large time delays $\Delta t > \Delta t_{max}$ with our theoretical model provides an estimate of the magnitude of the absorptive perturbation.

The best spatial resolution is observed, as expected, for shorter time-delays allowing one to determine the position of the tumor center on the 2-D image (transverse coordinates) with accuracy ~2.5 mm. After preliminary data processing that includes filtering and deconvolution of the raw time-resolved data, we created linear contrast scans passing through the tumor center and analyzed these scans, using our algorithm. Our estimates have shown that the tumor had larger absorption and scattering than the background. Estimated optical parameters of the tumor and the background tissue are summarized in Tables III and IV for patients #9 and #11, respectively.

Smaller number of available wavelengths (just two) comparing to a number of likely chromophores, mentioned above (not less than three) makes it impossible to fully determine the composition of the tumor and surrounding tissues. Assuming a relative content of water in the tissues of 30% and neglecting the contribution of lipids (that may be noticeable according to recent measurements (41)), preliminary estimates of tumor/tissue oxygenation and blood volume were made from this data that showed noticeable de-oxygenation of the tumors

Table III
Tumor parameters (patient # 9, assumed depth and size $\overline{z}$=53mm and d_f=26mm)

Estimated Parameters	λ=670nm	λ=785nm
μ_a (background)	0.0032 mm^{-1}	0.0028 mm^{-1}
μ_s' (background)	0.94 mm^{-1}	0.83 mm^{-1}
μ_a (target)	0.0080 mm^{-1}	0.0055 mm^{-1}
μ_s' (target)	1.48 mm^{-1}	1.15 mm^{-1}

Table IV
Tumor parameters (patient #11, assumed depth $\overline{z}$=15mm, estimated size d_f=23mm)

Estimated Parameters	λ=670nm	λ=785nm
μ_a (background)	0.0029 mm^{-1}	0.0024 mm^{-1}
μ_s' (background)	1.2 mm^{-1}	1.1 mm^{-1}
μ_a (target)	0.0071 mm^{-1}	0.0042 mm^{-1}
μ_s' (target)	1.76 mm^{-1}	1.6 mm^{-1}

relative to the surrounding tissue, combined with higher blood volume. In the case of patient #11 the results are less reliable due to the paucity of raw data for long time delays.

Analysis of two additional cases of invasive ductal carcinoma (patients #12, 16, not presented here) resulted in similar conclusions of higher blood content and lower oxygenation of tumors, relative to surrounding tissue. It is worth noting that scattering perturbation, related to the tumor, in some cases proved to be negative.

The reported results encouraged us to continue analysis of actual time-resolved measurements of human breast using our quantification methods to assess their ability to detect tumors and/or to provide spectroscopically identifiable physiological parameters (e.g., oxygenation, density, or water content) of tumors detected by other imaging modalities, in particular, for treatment monitoring in clinical trials.

Multi-wavelength system (more than two wavelengths) is required to estimate the blood oxygenation without *a priori* assumptions about the water content of the tissues, and such systems exist already (see e.g., (25)). Future research is aimed at collecting and analyzing new data sets of *in vivo* data, obtained from the red and near-infrared breast imaging of tissue abnormalities at different wavelengths (up to five), using methodology described above. The spectroscopic power of the time-resolved optical imaging system, along with our ability to quantify physiological parameters of human breast (such as, relative blood volume and blood oxygenation) prompted us to start collaboration with the Oncology Radiology Program at the National Cancer Institute, National Institutes of Health.

The new time-resolved optical mammograph, build by a Canadian based company, *Advanced Research Technology (ART)*, will be installed at the NIH campus. Our goals are to extend our knowledge about the physiological properties of breast cancer with regard to oxygenation and vascular density by optical determination. This will allow us to determine how optically derivable parameters of known breast cancers correlate with biological measurements of the tumor specimens, and how such correlation compares with other imaging modalities like MRI and PET. In the course of our study we will determine whether changes in the optical parameters over several measurements prior to and during radio and/or chemotherapy correlates with response. Finally, we will be able to evaluate the role that optically derivable parameters may play with respect to therapy stratification for neoadjuvant therapies by establishing correlations to existing prognostic factors and to therapy results.

Quantitative Fluorescence Imaging

Rationale

Fluorescence properties of biomolecules, along with the development of specific exogenous cell surface markers have been the critical cornerstone of successes of modern molecular biology. The new challenge is how these powerful techniques can be used *in vivo*. In cancer research, quantitative and specific non-invasive or minimally invasive methods are desired.

If successful, noninvasive "optical biopsies" may replace invasive, destructive biopsies and provide the advantages of smaller sampling errors and reduction in cost and time for diagnosis. This will result in better integration of diagnosis and therapy by tracking progression of disease or its regression in response to therapy. Sequential temporal analysis of fluorescence signal could also provide dynamic follow-up of these specific markers as seen in fMRI setting.

Clinically practical fluorescence imaging techniques must meet several requirements. First, the pathology under investigation must not lie at a depth where the attenuation of the signal results in a poor signal-to-noise ratio and poor resolvability. Second, the specificity of the marker must be high enough that one can clearly distinguish between normal tissue and lesions. Finally, one must have a robust image reconstruction algorithm which enables one to quantify the fluorophore concentration at the site of the lesion.

In *Theory and 3-D Reconstruction Algorithm*, the general quantitative theory of diffuse fluorescence imaging and its substantiation with phantom experiments will be presented. An animal model to study the immune response to tumor, using quantitative diffuse fluorescence imaging will be discussed. Potential use of life-times of fluorescence molecules as another specific tool for non-invasive monitoring of tumors will be presented in ***Fluorescence Lifetime as a Potential Tool for Functional Imaging***.

Theory and 3-D Reconstruction Algorithm

The fluorescent image observed at the tissue surface is not only dependent on the concentration of the fluorophore, but is closely dependent on the optical properties of the tissue at the excitation and emission wavelengths of the fluorescent mass and its location. Therefore, for quantitative analysis one should describe photon paths in to the tissue. We have devised a general theory of diffuse fluorescence photon migration based on RWT. In the probabilistic RWT model, the description of a photon path may be divided into three parts: the path from the photon source to a localized, fluorescing target; the interaction of the photon with the fluorophore; and finally, the path of the fluorescently emitted photon to a detector. Each part of the photon path may be described by a probability: first, the probability that an incident photon will arrive at the fluorophore site; second, the probability that the photon has a reactive encounter with the fluorophore and the corresponding photon transit delay, which is dependent on the lifetime of the fluorophore, and the probability of the fluorophore emitting a photon; and third, the probability that the photon emitted by the fluorophore travels from the reaction site to the detector. Each of these three sequences is governed by a stochastic process.

For the purpose of our research, we have derived an analytical expression for CW imaging in the reflectance mode (42, 43). The probability of detecting an emitted photon ($\Gamma(\mathbf{r},\mathbf{s})$), originating at the deeply embedded fluorophore, is given by a random walk formula (42, 44):

$$\Gamma(\mathbf{r},\mathbf{s}) = \frac{\Phi \frac{\mu_{af}}{\mu'_{sf}} [H(\alpha_-,\beta_-) - H(\alpha_-,\beta_+) - H(\alpha_+,\beta_-) + H(\alpha_+,\beta_+)] \exp(-\frac{\mu_{ae}}{\mu'_{se}})}{\left\{1 - \frac{\mu_{af}}{\mu'_{sf}} + \frac{\mu_{af}}{\mu'_{sf}} \left[1 + \frac{1}{8}\left(\frac{3}{\pi}\right)^{3/2} \sum_{m=1}^{\infty} \frac{1}{m^{3/2}} \exp(-2m\frac{\mu_{ai}}{\mu'_{si}})\right]\right\}}, \quad [3]$$

Where:

$$H(\alpha,\beta) = \frac{1}{\sqrt{\alpha\beta}} \exp\left\{-2\left[\sqrt{\alpha}\,\frac{\mu_{ai}}{\mu'_{si}} + \sqrt{\beta}\,\frac{\mu_{ae}}{\mu'_{se}}\right]\right\}, \quad [4]$$

$$\alpha_{\pm} = \frac{3}{4}\left[\bar{x}_f^2 + \bar{y}_f^2 + (\bar{z}_f \pm \frac{\sqrt{2}}{\mu'_{si}})^2\right]\mu'^{2}_{si} \quad [5]$$

and

$$\beta_{\pm} = \frac{3}{4}\left[(\bar{x}_f - \bar{x})^2 + (\bar{y}_f - \bar{y})^2 + (\bar{z}_f + \frac{\sqrt{2}}{\mu'_{se}} \pm \frac{\sqrt{2}}{\mu'_{se}})^2\right]\mu'_{se} \quad [6]$$

Here, the origin of the coordinate system (0,0,0) is placed at the entry point of the incident photon, and the coordinates of the fluorescent site and the detector are $(\bar{x}_f, \bar{y}_f, \bar{z}_f)$ and $(\bar{x}, \bar{y}, \bar{z})$ respectively. The optical parameters in this equation, μ'_s and μ'_a, are the background's transport-corrected scattering and absorption coefficients, respectively. The subscripts i and e stand for incident and emitted light. Symbols μ'_{sf} and μ_{af} represent the optical characteristics (i.e., the transport-corrected scattering and absorption coefficients, respectively) of the fluorescent site. The parameter Φ (so-called quantum efficiency) is the probability that an excited fluorophore will, in fact, emit a fluorescent photon. It should be noted that for several fluorescent sites, the detected signal can be considered as the sum of the signals arising from individual fluorophores. The accuracy of our theoretical findings has been tested in wide range of phantom experiments.

The next step is to devise an inverse algorithm which enables one to find the location of the fluorescent mass and its concentration. The observed 2-D intensity distributions of the emitted light were normalized to the maximum intensity measured in the experiment and used as an input data for 3-D localization of the target.

Our analysis is based on a comparison of measured fluorescent intensity distributions with the theoretical expression for the probability $\Gamma(\mathbf{r},\mathbf{s})$ (Eq. 3) that corresponds to the intensity distribution of the light emitted by a fluorophore embedded at a given depth. Parameters μ'_{sf} and μ_{af}, and the whole denominator of the RHS of Eq. [3] are not required for the reconstruction because they determine only the scaling of the intensities.

The algorithm uses a multi-parameter curve fitting procedure, based on a standard Levenberg-Marquardt method (14). The 2-D problem is reduced to 1-D using a single variable $w = (x/s)n_{sc} + y/s$ that characterizes the position of the pixel on the image plane, where s is the distance between neighboring pixels and n_{sc} is the number of pixels in each linear scan (e.g., $n_{sc} = 512$ for a square image field of 512×512 pixels). The strong dependence of the intensity distributions (given by Eq. [3]) on the fluorophore depth contributes to the robustness of the algorithm (44). This algorithm also has been tested in well define phantoms (45).

Animal Model

In order to further improve our reconstruction method and make it a general tool for optical biopsy we have created an animal model – mice with SQCC in their oral cavity. This model is very repeatable and could be used by us for further investigations and refinement of our model. The aim is to follow the immune response to tumor cells.

A set of 50 BALB/c mice was divided into control and experimental groups. The experimental group was injected, into the tongue with 50 µl of the SqCC cell line. At various time intervals, ranging from one to 20 days after cell-line injection a sub-group (comprising 5 experimental and 2 control mice) was anesthetized and injected into the tongue, with 50 µl of either anti-CD3-FITC or anti-CD19-FITC conjugates (Southern Biotechnology, CA, USA). These antibodies were chosen for conjugation with the FITC fluorescent marker since the SqCC cell line is associated with massive infiltration of CD3- and CD19-positive cells into the tumor area (46). This procedure was repeated 1, 2, 5, 8, 14 and 20 days after cell-line injection.

In order to simulate the location of tumors at various depths (to maximum of 2 mm), we covered each tongue with an appropriate thickness of agarose slab (to simulate a tumor at greater depth). The tongues were then excited by Argon laser at 488 nm (optimized to the FITC absorption line). The optical system set-up is illustrated in Figure 9. The laser beam was directed to the tissue through sets of reflecting mirrors. The anesthetized mouse was held on a custom-designed device (to avoid movement of the head) mounted on a XYZ positioner. The emitted fluorescent light (520-550 nm) was limited by special band pass filters and a dichroic mirror. The filter and the reverse side of the dichroic mirror suppress the laser signal while being transparent to the returning fluorescence signal, which was collected by a high precision fluorescence camera. Immediately thereafter, the tongues were excised, fixed in formalin, and embedded in paraffin.

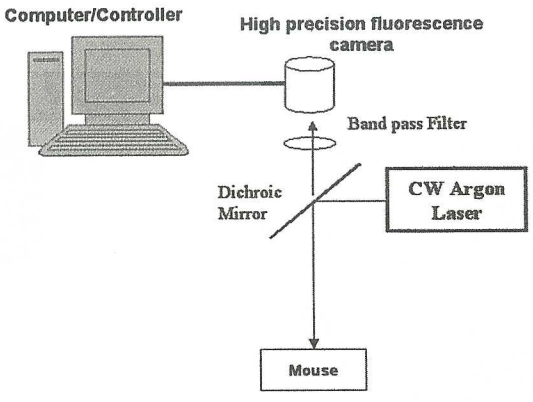

Figure 9: Fluorescent imaging experimental set up.

Sections (4 µm thick) were prepared and stained with Haematoxilin and Eosin (H&E). Morphological features were then identified. Figure 10 is an H&E staining of a section obtained from the tongue of a diseased mouse 2 days after injection of the cell line. One sample, out of the whole set of fluorescence images obtained, is shown in Figure 11.

In our experiments we observed formation and development of a single fluorescent object, localized in the tumor area. In this case the fitting parameters are the coordinates of the fluorophore in question and the background intensity. *A priori* known values are the field-of-view dimensions (i.e., number of pixels along each axis) and inter-pixel distance (scanning step). To start the reconstruction, initial values for the background optical parameters (μ_{si}', μ_{ai}, and μ_{se}', μ_{ae} at the excitation and emission wavelengths) were chosen from the measurements of total reflectance and transmittance obtained by the integrating spheres method (45). A Comparison of the detected intensity profiles with the profiles reconstructed from the theoretical model is shown in Figure 12.

The next step in our research, which we are currently working on, is the study of the pharmacokinetics of fluorophore-antibody in the vicinity of tumor. This study should assist us in determining when specific binding to tumor antigens occurs and when all other markers have diffused away. At this stage, one should image the fluorescence for localization. We started this study by taking only peak fluorescence measurements with spectrophotometers and looking at the decrease in the peak as a function of time. The washout was compared between healthy *in vivo* tissue and sick *in vivo* tissue (47). Figure 13 exhibits the difference between the two cases.

In our current pharmacokinetics study we have taken fluorescence images of the tissue. Then we take a cross-sectional slice through the peak fluorescence and look at the broadening of the fluorescence signal as a function of time (48). Figure 14 is an example of clearance time as seen through an agarose slab (to simulate a tumor at greater depth) and deconvolved to show actual exponential clearance of fluoresceinated antibodies in the vicinity of a tumor in mouse tissue.

Fluorescence Lifetime as a Potential Tool for Functional Imaging

It is well established today that several important properties of tumors *in vivo* differ in value from normal tissue properties. Some of these changes are extracellular pH (pHe) distribution, blood flow, tissue oxygen and nutrient supply, bioenergetic status and temperature. Some of these changes are derived from the heterogeneity in tumor vascularization (49), which leads also to a reduction in the efficiency of disposal of waste products (e.g., hydrogen ions, lactic acid, necrosis products etc.). These changes can be useful tools in

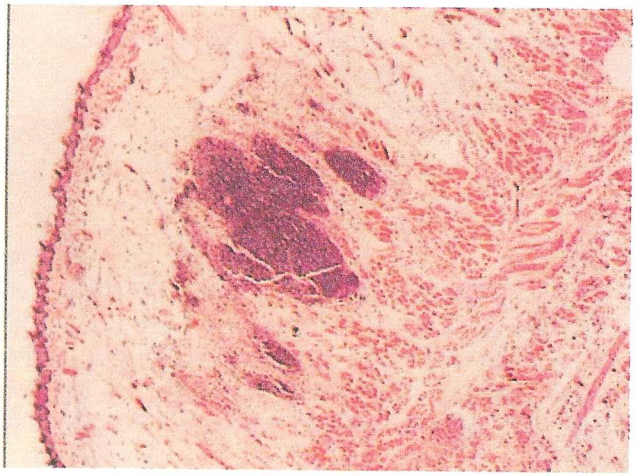

Figure 10: H&E staining of a 2 days old tumor.

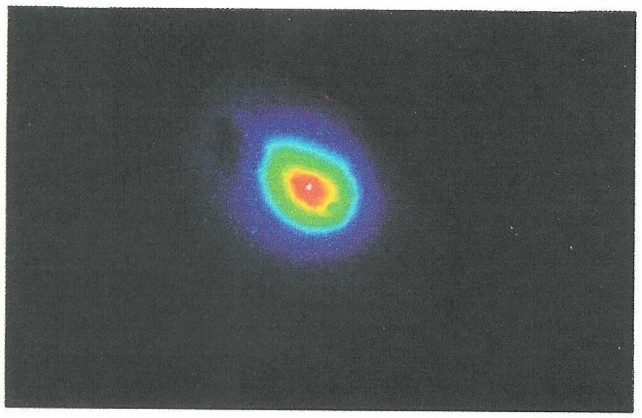

Figure 11: Surface fluorescence image of a tumor marked with fluoreceinated antibody in mouse model.

prognosis of malignancies and in the development of techniques for drug targeting in tumors. This introduction will focus on the altered properties (mainly pH and thermo-tolerance) as indicators in the diagnosis of tumors.

In a tumor microenvironment, pHe tends to exhibit a more acidic value than that of normal tissue. This property, referred to as acidosis, is thought to be due to a high metabolic rate in a rapidly growing tumor (either glycolytic or lactic acid production), accompanied by an insufficient drainage by convective and/or diffusive transport. Thus, while the intracellular pH is maintained at a more physiologically normal pH by self regulating systems such as using ion exchangers Na^+/H^+ antiport and Na^+-dependent $HCO3^-/Cl^-$ exchanger, the extracellular matrix in a tumor becomes more acidic than normal, creating a pH gradient inversed to the normal state (in which pHe is less acidic) (50, 51).

The pHe in many solid tumors exhibits a low value that can decrease to 5.6 in contrast to the pHe range in normal tissue of 7.2-7.6 (52). The average decrease in pHe is 0.3-0.5 pH units.

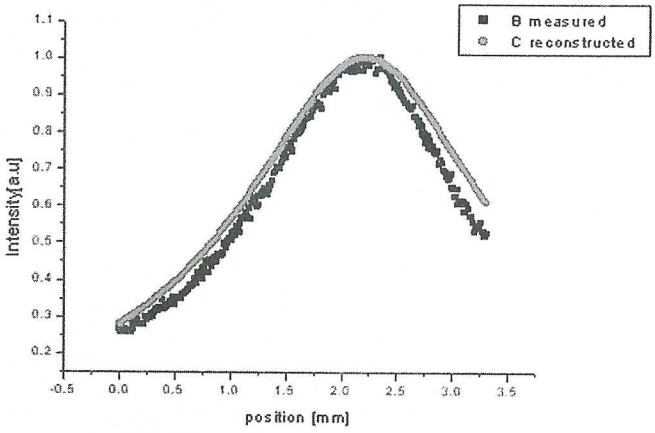

Figure 12: Comparison of the detected intensity profiles with the profiles, reconstructed from the theoretical model. (Taken at day 2). Sick mouse, for z_f = 1.18 mm nominal thickness of the turbid layer above the mouse tongue with Antibody+fluorophore. Reconstructed depth 1.09 mm.

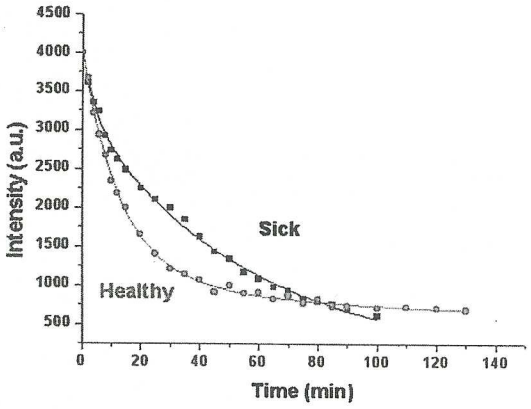

Figure 13: Comparison of peak fluorescence decay curves of healthy and sick mouse.

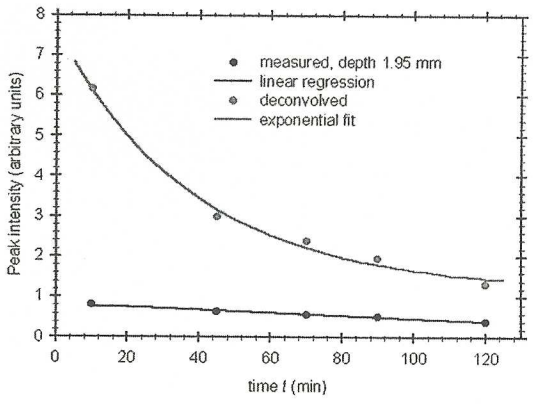

Figure 14: Clearance time as seen through a slab and deconvolved to show actual exponential clearance.

When pH measurements were taken in various studies in animal models with human tumors and in a variety of human tumors (53, 54), the findings clearly showed that there was a positive correlation between the tumor size and the decrease in pHe. A decrease in pHe was detected even in small tumors.

The measurement methods used in research vary from pH-sensitive mini/microelectrodes (53), to a PET-based technique, and ^{1}H NMR spectroscopy using ^{31}P and ^{19}F as probes (55). These methods are either invasive or involve the use of harmful materials for the measurement procedure.

Tumor temperature is usually higher than in surrounding normal tissue (56). The rapid growth of vascularized tissue mass at a relatively high temperature and a high heat dissipation capacity (because of the large blood perfusion rates) is one of the main causes for this regional hyperthermia, and, in fact, several investigators have used ultrasound and other methods to prove that blood flow is higher inside a malignant tumor (57). In general, it is found that tumor temperature is 0.5-4.0° C higher than that of the normal tissue (58). Additionally, neoplastic tissue also exhibits a different response from normal tissue during hyperthermia (59).

When investigating the existence of a thermal distinction between malignant tumors and inflammatory benign lesions (60) using thermometric measurements, a positive correlation was found between Δtemperature and degree of angiogenesis. Temperatures greater than 1° C above the surrounding tissue can indicate a malignant tumor and an increase of one additional degree triples the odds of a patient having a malignant tumor.

Theory of Fluorescence Lifetime

In vivo measurements of tumor pHe or temperature generally require the invasive insertion of needle probes. Some fluorophores, however, have a known dependence between their decay lifetime and environmental parameters such as temperature and pH (61). The use of such probes has been demonstrated using microscopy on thin, transparent samples (61). In such case, the fluorophore lifetime may be measured by fitting time-resolved measurements of intensity following a brief exciting pulse of light to an exponential decay function, or by using a frequency-modulated source and transforming the results to the time domain. Extending the utility of fluorescence lifetime to *in vivo* applications requires a different approach. The highly scattering nature of tissue causes dispersion in the time of arrival of photons traveling through tissue that mimics the delay at a fluorescent site. Thus, the two sources of dispersion must be isolated. Several researchers have used a diffusion-approximation to transport theory-based method of separating the components using frequency-resolved measurements (7, 62, 63).

Random walk theory has been used to create a model that allows one to separate a lifetime component from path length dispersion (64) for time-resolved measurements in inhomogeneous media. The probability of a fluorescence photon arriving at a detector is:

$$y(t) = \frac{\mu_{af}}{\mu_{si}'} \Phi \left[W_t - \langle \Delta t \rangle \frac{dW_t}{dt} \right] \qquad [7]$$

Where μ_{af} is the component of the coefficient of absorption which is due to the presence of fluorophores and μ_{af} is a function of fluorophore concentration, μ_{si}' is the transport-corrected scattering at the excitation wavelength, Φ is the quantum efficiency of the fluorophore, and $\langle \Delta t \rangle$ is the mean time delay due to a fluorescence event. W_t has been shown to be analogous to a point-spread function (see *Theoretical Model and Phantom Experiments*) and, for highly scattering media, is a function of time and is dependent on the scattering coefficient, as well as the geometry of the source, fluorophore and detector (64). Eq. [7] shows that the effect of the fluorescent delay is proportional to the time-derivative of the point-spread function. Additionally, an underlying assumption is that $\langle \Delta t \rangle$ be comparable or smaller than photon transit times from the source, through the fluorophore site and finally to the detector.

From Eq. [7], it has been shown that the time-resolved fluorescence contrast between two measurements taken on the surface of scattering media may be expressed as follows (64):

$$C = \frac{(\langle \tau \rangle - \tau_s)}{p_t} \frac{dW_t}{dt} \qquad [8]$$

where $\langle \tau \rangle$ is the mean lifetime of the tissue and τ_s is the perturbed lifetime at a potential tumor site, p_t, is the probability of a photon arriving at the measurement site and passing through the fluorophore site, but absent any fluorescent behavior. The value of p_t may be approximated from measurements of intensity at the excitation wavelength. The last factor, dW_t/dt, because it is very dependent on position, may be viewed as a spatial filter. For a given source-detector geometry, by selecting specific values of dW_t/dt, which correspond to specific depths in the tissue, the lifetime perturbation at specific depths may be estimated even when the lifetime is spatially inhomogeneous (64).

To substantiate our theory, we have designed tissue-like phantoms with Agarose based gels, containing 1.7% Intralipid as the scattering medium. pH is controlled via choosing the desired buffer solution as the liquid medium when preparing the gel. Temperature is controlled via placing the sample on a small heating plate regulated by a PID temperature controller. A desired concentration of the fluorescent marker (absorbs and emits in the NIR region) is

achieved using non-diffusing 6 μm diameter beads to which the marker is conjugated.

The experimental set-up shown in Figure 15 uses a Titanium:Sapphire mode-locked laser (80MHz) as the light source (Spectra-Physics Lasers, USA), a fast photodiode for laser synchronization, a fast photomultiplier tube as the detector and fluorescence collection optics. A complete Time-Correlated Single Photon Counting system is integrated on a PC board and controlled through a software (Becker & Hickl GmbH, Germany) to record fluorescence decay curves. pH and temperature data is measured for reference using 100 μm glass tip electrodes (Unisense, Denmark).

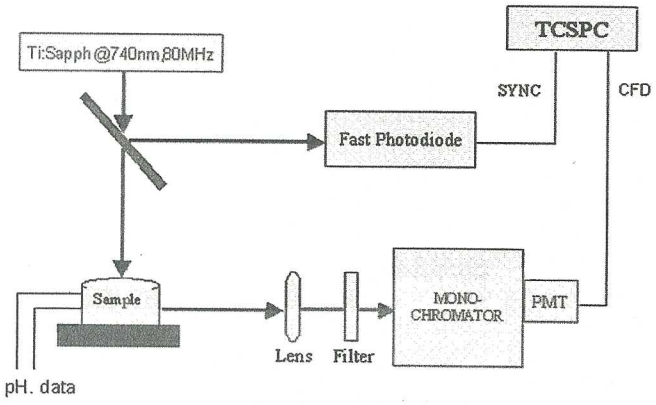

Figure 15: Experimental set-up to measure fluorescence decay curves in phantoms as function of source detector separation, depth of fluorescent markers and changes in pH.

A set of experiments were designed to study the effects of differing parameters on the detected signal. Source-detector separation dependence, depth dependence, and variation of pH were systematically studied. An example of a good agreement between phantom experiment and our theory at pH = 7 is shown in Figure 16.

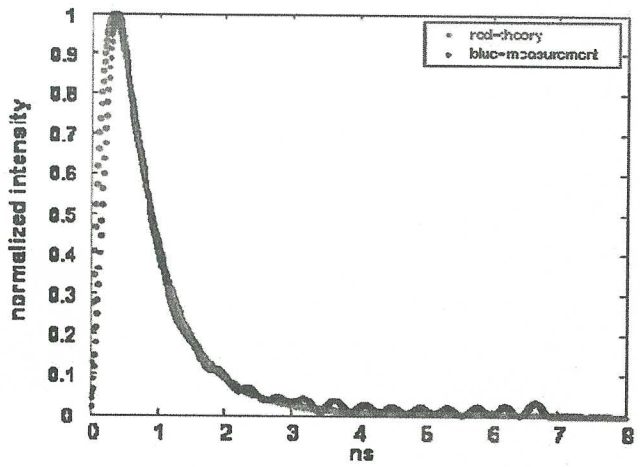

Figure 16: Comparison of theory vs. measurement for a 5mm flurophore depth, at pH = 7.

Our future studies involved with testing our inverse method sensitivity to differences in pH. Introduction of temperature changes in the phantom model. Embedding cell-lines and markers into the phantoms and measure dependence of fluorescence decay time as a function of pH and temperature and then move into animal models with induced tumors in them.

Conclusions

The spectroscopic capabilities of light have played a critical role in the advance of knowledge in biology and medicine. With the advent of molecular based medicine, the "natural" method of non-invasively characterizing cell and tissue abnormalities *in vivo* is through the use of this capability. However, quantification of physiological parameters below the tissue surface is not straightforward. A complex analytical process is needed to take into account the effects of scattering.

Optical imaging techniques applied to deep tissue structures suffer from inherent low resolution. It is possible to overcome this disadvantage by using a combination of modalities; for example: CT or MRI which provides high resolution structural images combined with optical spectroscopy which provides biochemical specificity. New contrast agents with new biochemical specificities are constantly being developed which will make optical methods increasingly valuable. The biomedical optics research community should concentrate its efforts on devising related image analysis techniques, designing appropriate hardware technologies, and finally studying the pharmacokinetics of various agents (therapeutics or diagnostics) to make biomedical optics more clinically relevant and move quantitative functional optical imaging methods to the patient's bedside.

Acknowledgment

Our special thanks go to Professor Rinneberg at PTB, Germany, who provided clinical data for our breast project. Special thanks also to Dr. Gallya Gannot from NIH/NCI for valuable data on the immune system response to the mice tumors and on creation of those animal models. Thanks also to Ms. Avital Garashi for taking part in the CW fluorescence imaging part and to Mr. Izhar Ron for his part in the fluorescence lifetime project.

References

1. Taroni, P., Pifferi, A., Torricelli, A., Cubeddu, R. Time-resolved Spectroscopy and Imaging in Diffusive Media Applied to Medical Diagnostics. *Rivista Del Nuovo Cimento 25*, 1-19 (2002).
2. Saidi, I. S., Jacques, S. L., Tittel, F. K. Mie and Rayleigh Modeling of Visible-Light Scattering in Neonatal Skin. *Applied Optics 34*, 7410-7418 (1995).
3. Marchesini, R., Bertoni, A., Andreola, S., Melloni, E., Sichirollo, A. E. Extinction and Absorption-Coefficients and Scattering Phase Functions of Human-Tissues *In Vitro*. *Applied Optics 28*, 2318-2324 (1989).

4. Gandjbakhche, A. H., Nossal, R., Bonner, R. F. Scaling Relationships for Theories of Anisotropic Random-Walks Applied to Tissue Optics. *Applied Optics 32*, 504-516 (1993).
5. Weissleder, R. A Clearer Vision for *In Vivo* Imaging. *Nature Biotechnology 19*, 316-317 (2001).
6. Kamalov, V. F., Struganova, I. A., Yoshihara, K. Temperature Dependent Radiative Lifetime of J-aggregates. *Journal of Physical Chemistry 100*, 8640-8644 (1996).
7. Hutchinson, C. L., Lakowicz, J. R., Sevickmuraca, E. M. Fluorescence Lifetime-Based Sensing in Tissues – A Computational Study. *Biophysical Journal 68*, 1574-1582 (1995).
8. Mordon, S., Devoisselle, J. M., Maunoury, V. *In Vivo* Ph Measurement and Imaging of Tumor-Tissue Using a Ph- Sensitive Fluorescent-Probe (5,6-Carboxyfluorescein) – Instrumental and Experimental Studies. *Photochemistry and Photobiology 60*, 274-279 (1994).
9. Alveryd, A., Andersson, I., Aspegren, K., Balldin, G., Bjurstam, N., Edstrom, G., Fagerberg, G., Glas, U., Jarlman, O., Larsson, S. A., Lidbrink, E., Lingaas, H., Lofgren, M., Rudenstam, C. M., Strender, L., Samuelsson, L., Tabar, L., Taube, A., Wallberg, H., Akesson, P., Hallberg, D. Lightscanning Versus Mammography for the Detection of Breast Cancer in Screening and Clinical-Practice – A Swedish Multicenter Study. *Cancer 65*, 1671-1677 (1990).
10. Nioka, S., Miwa, M., Orel, S., Schnall, M., Haida, M., Zhao, S., Chance, B. Optical Imaging of Human Breast Cancer. *Adv. Exp. Med. Biol. 361*, 171-179 (1994).
11. Franceschini, M. A., Moesta, K. T., Fantini, S., Gaida, G., Gratton, E., Jess, H., Mantulin, W. W., Seeber, M., Schlag, P. M., Kaschke, M. Frequency-domain Techniques Enhance Optical Mammography: Initial Clinical Results. *Proceedings of the National Academy of Sciences of the United States of America 94*, 6468-6473 (1997).
12. Troy, T. L., Page, D. L., Sevick-Muraca, E. Optical Properties of Normal and Diseased Breast Tissues: Prognosis for Optical Mammography. *Journal of Biomedical Optics 1*, 342-355 (1996).
13. Grosenick, D., Wabnitz, H., Rinneberg, H. H., Moesta, K. T., Schlag, P. M. Development of a Time-domain Optical Mammograph and First *In Vivo* Applications. *Applied Optics 38*, 2927-2943 (1999).
14. Henson, D. E., Ries, L., Freedman, L. S., Carriaga, M. Relationship Among Outcome, Stage of Disease, and Histologic Grade for 22,616 Cases of Breast Cancer – The Basis for a Prognostic Index. *Cancer, 68*, 2142-2149 (1991).
15. Winchester, D. J., Menck, H. R., Winchester, D. P. National Treatment Trends for Ductal Carcinoma *In Situ* of the Breast. *Archives of Surgery 132*, 660-665 (1997).
16. Hebden, J. C., Arridge, S. R., Delpy, D. T. Optical Imaging in Medicine: I. Experimental Techniques. *Physics in Medicine and Biology 42*, 825-840 (1997).
17. Cutler, M. Transillumination as an Aid in the Diagnosis of Breast Lesions. *Surg. Gynecol. Obstet., 48*, 721-728 (1929).
18. Monsees, B., Destouet, J. M., Gersell, D. Light Scan Evaluation of Nonpalpable Breast Lesions. *Radiology 163*, 467-470 (1987).
19. Chance, B., Leigh, J. S., Miyake, H., Smith, D. S., Nioka, S., Greenfeld, R., Finander, M., Kaufmann, K., Levy, W., Young, M., Cohen, P., Yoshioka, H., Boretsky, R. Comparison of Time-Resolved and Time-Unresolved Measurements of Deoxyhemoglobin in Brain. *Proceedings of the National Academy of Sciences of the United States of America 85*, 4971-4975 (1988).
20. Delpy, D. T., Cope, M., Vanderzee, P., Arridge, S., Wray, S., Wyatt, J. Estimation of Optical Pathlength Through Tissue from Direct Time of Flight Measurement. *Physics in Medicine and Biology 33*, 1433-1442 (1988).
21. Patterson, M. S., Chance, B., Wilson, B. C. Time Resolved Reflectance and Transmittance for the Noninvasive Measurement of Tissue Optical-Properties. *Applied Optics 28*, 2331-2336 (1989).
22. Nossal, R., Bonner, R. F., Weiss, G. H. Influence of Path-Length on Remote Optical Sensing of Properties of Biological Tissue. *Applied Optics 28*, 2238-2244 (1989).
23. Benaron, D. A., Stevenson, D. K. Optical Time-of-Flight and Absorbency Imaging of Biologic Media. *Science 259*, 1463-1466 (1993).
24. Grosenick, D., Moesta, K. T., Wabnitz, H., Mucke, J., Stroszczynski, C., Macdonald, R., Schlag, P. M., Rinneberg, H. Time-domain Optical Mammography: Initial Clinical Results on Detection and Characterization of Breast Tumors. *Applied Optics 42*, 3170-3186 (2003).
25. Pifferi, A., Taroni, P., Torricelli, A., Messina, F., Cubeddu, R., Danesini, G. Four-wavelength Time-resolved Optical Mammography in the 680-980 nm Range. *Optics Letters 28*, 1138-1140 (2003).
26. Arridge, S. R., Hebden, J. C. Optical Imaging in Medicine: II. Modelling and Reconstruction. *Physics in Medicine and Biology 42*, 841-853 (1997).
27. Gandjbakhche, A. H., Weiss, G. H., Bonner, R. F., Nossal, R. Photon Path-Length Distributions for Transmission Through Optically Turbid Slabs. *Physical Review E 48*, 810-818 (1993).
28. Alfano, R. R. Optical Biopsy IV in *Photonics West*. San-Jose: SPIE (2002).
29. Weissleder, R. Scaling Down Imaging: Molecular Mapping of Cancer in Mice. *Nature Reviews Cancer 2*, 11-18 (2002).
30. Gandjbakhche, A. H., Nossal, R., Bonner, R. F. Resolution Limits for Optical Transillumination of Abnormalities Embedded in Tissues. *Medical Physics 22*, 185-191 (1994).
31. Gandjbakhche, A. H., Bonner, R. F., Nossal, R., Weiss, G. H. Absorptivity Contrast in Transillumination Imaging of Tissue Abnormalities. *Applied Optics 35*, 1767-1774 (1996).
32. Chernomordik, V., Hattery, D. W., Gannot, I., Zaccanti, G., Gandjbakhche, A. Analytical Calculation of the Mean Time Spent by Photons Inside an Absorptive Inclusion Embedded in a Highly Scattering Medium. *Journal of Biomedical Optics 7*, 486-492 (2002).
33. Chernomordik, V., Hattery, D., Gandjbakhche, A. H., Pifferi, A., Taroni, P., Torricelli, A., Valentini, G., Cubeddu, R. Quantification by Random Walk of the Optical Parameters of Nonlocalized Abnormalities Embedded within Tissuelike Phantoms. *Optics Letters 25*, 951-953 (2000).
34. Gandjbakhche, A. H., Chernomordik, V., Hebden, J. C., Nossal, R. Time-dependent Contrast Functions for Quantitative Imaging in time-resolved Transillumination Experiments. *Applied Optics 37*, 1973-1981 (1998).
35. Tromberg, B. J., Coquoz, O., Fishkin, J., Pham, T., Anderson, E. R., Butler, J., Cahn, M., Gross, J. D., Venugopalan, V., Pham, D. Non-invasive Measurements of Breast Tissue Optical Properties Using Frequency-domain Photon Migration. *Philosophical Transactions of the Royal Society of London Series B-Biological Sciences 352*, 661-668 (1997).
36. Tromberg, B. J., Shah, N., Lanning, R., Cerussi, A., Espinoza, J., Pham, T., Svaasand, L., Butler, J. Non-invasive *In Vivo* Characterization of Breast Tumors Using Photon Migration Spectroscopy. *Neoplasia 2*, 26-40 (2000).
37. Fantini, S., Walker, S. A., Franceschini, M. A., Kaschke, M., Schlag, P. M., Moesta, K. T. Assessment of the Size, Position, and Optical Properties of Breast Tumors *In Vivo* by Noninvasive Optical Methods. *Applied Optics 37*, 1982-1989 (1998).
38. Press, W. H., Teukolsky, S., Vetterling, W. T., Flannery, B. P., *Numerical Recipes in C: The Art of Scientific Computing. 2nd Ed.* pp. 994. Cambridge; New York: Cambridge University Press (1992).
39. Wabnitz, H.,Rinneberg, H. Imaging in Turbid Media by Photon Density Waves: Spatial Resolution and Scaling Relations. *Applied Optics 36*, 64-74 (1997).
40. Sevick, E. M., Chance, B., Leigh, J., Nioka, S., Maris, M. Quantitation of Time-Resolved and Frequency-Resolved Optical-Spectra for the Determination of Tissue Oxygenation. *Analytical*

Biochemistry 195, 330-351 (1991).
41. Taroni, P., Pifferi, A., Torricelli, A., Comelli, D., Cubeddu, R. *In Vivo* Absorption and Scattering Spectroscopy of Biological Tissues. *Photochemical & Photobiological Sciences 2*, 124-129 (2003).
42. Gandjbakhche, A. H., Bonner, R. F., Nossal, R., Weiss, G. H. Effects of Multiple-passage Probabilities on Fluorescent Signals from Biological Media. *Applied Optics 36*, 4613-4619 (1997).
43. Gandjbakhche, A. H.,Gannot, I. Quantitative Fluorescent Imaging of Specific Markers of Diseased Tissue. *Ieee Journal of Selected Topics in Quantum Electronics 2*, 914-921 (1996).
44. Chernomordik, V., Hattery, D., Gannot, I., Gandjbakhche, A. H. Inverse Method 3-D Reconstruction of Localized *In Vivo* Fluorescence – Application to Sjogren Syndrome. *Ieee Journal of Selected Topics in Quantum Electronics 5*, 930-935 (1999).
45. Gannot, I., Bonner, R. F., Gannot, G., Fox, P. C., Smith, P. D., Gandjbakhche, A. H. Optical Simulations of a Noninvasive Technique for the Diagnosis of Diseased Salivary Glands *In Situ*. *Medical Physics 25*, 1139-1144 (1998).
46. Gannot, G., Gannot, I., Vered, H., Buchner, A., Keisari, Y. Increase in Immune Cell Infiltration with Progression of Oral Epithelium from Hyperkeratosis to Dysplasia and Carcinoma. *British Journal of Cancer 86*, 1444-1448 (2002).
47. Gannot, I., Gannot, G., Garashi, A., Gandjbakhche, A., Buchner, A., Keisari, Y. Laser Activated Fluorescence Measurements and Morphological Features - An *In Vivo* Study of Clearance Time of FITC Tagged Cell Markers. *Journal of Biomedical Optics 7*, 14-19 (2002).
48. Gannot, I., Garashi, A., Gannot, G., Chernomordik, V., Gandjbakhche, A. *In Vivo* Quantitative 3-D Localization of Tumor Labeled with Exogenous Specific Fluorescence Markers. *Applied Optics 42*, in press (2003).
49. Vaupel, P., Kallinowski, F., Okunieff, P. Blood Flow, Oxygen and Nutrient Supply, and Metabolic Microenvironment of Human Tumors: A Review. *Cancer Research 49*, 6449-6465 (1989).
50. Boyer, M. J.,Tannock, I. F. Regulation of Intracellular pH in Tumor Cell Line: Influence of Microenvironmental Conditions. *Cancer Research 52*, 4441-4447 (1992).
51. Wahl, M. L., Pooler, P. M., Briand, P., Leeper, D. B., Owen, C. S. Intracellular pH Regulation in a Nonmalignant and a Derived Malignant Human Breast Cell Line. *Journal Of Cellular Physiology 183*, 373-380 (2000).
52. Griffiths, J. R. Are Cancer Cells Acidic. *British Journal of Cancer 64*, 425-427 (1991).

Date Received: October 15, 2003

53. Engin, K., Leeper, D. B., Cater, J. R., Thistlethwaite, A. J., Tupchong, L., Mcfarlane, J. D. Extracellular pH Distribution in Human Tumors. *Int. J. Hyperthermia 11*, 211-216 (1995).
54. Kallinowski, F.,Vaupel, P. pH Distributions in Spontaneous and Isotransplanted Rat Tumors. *British Journal of Cancer 58*, 314-321 (1988).
55. Garcia-Martin, M. L., Herigault, G., Remy, C., Farion, R., Ballesteros, P., Coles, J. A., Cerdan, S., Ziegler, A. Mapping Extracellular pH in Rat Brain Gliomas *In Vivo* by 1H Magnetic Resonance Spectroscopic Imaging: Comparison with Maps of Metabolites. *Cancer Research 61*, 6524-6531 (2001).
56. Gautherie, M. Thermopathology of Breast Cancer: Measurement and Analysis of *In Vivo* Temperature and Blood Flow. *Ann. NY Acad. Sci 335*, 383-413 (1980).
57. Gullino, P. M. Influence of Blood Supply on Thermal Properties and Metabolism of Mammary Carcinomas. *Ann. NY Acad. Sci*, 1-17 (1980).
58. Pierart, J., Burmeister, R., Steinberg, J., Schalper, J., Cid, L. of Thermography in the Differential Diagnosis of Phylloides Tumour. *British Journal of Surgery 77*, 783-784 (1990).
59. Jain, R. K. Temperature Distributions in Normal and Neoplastic Tissues During Normothermia and Hyperthermia. *NY Acad. Sci 335*, 48-62 (1980).
60. Stefanadis, C., Chrysochoou, C., Markou, D., Petraki, K., Panagiotakos, D. B., Fasoulakis, C., Kyriakidis, A., Papadimitriou, C., Toutouzas, P. K. Increased Temperature of Malignant Urinary Bladder Tumors *In Vivo*: The Application of a New Method Baesd on a Catheter Technique. *Journal of Clinical Oncology 19*, 676-681 (2001).
61. Andersson, R. M., Carlsson, K., Liljeborg, A., Brismar, H. Characterization of Probe Binding and Comparison of its Influence on Fluorescence Lifetime of Two pH-sensitive Benzo[c]xanthene Dyes using Intensity-modulated Multiple-wavelength Scanning Technique. *Anal Biochem 283*, 104-10 (2000).
62. Jiang, H. B. Frequency-domain Fluorescent Diffusion Tomography: A Finite Element-based Algorithm and Simulations. *Applied Optics 37*, 5337-5343 (1998).
63. Reynolds, J. S., Troy, T. L., Mayer, R. H., Thompson, A. B., Waters, D. J., Cornell, K. K., Snyder, P. W., Sevick-Muraca, E. M. Imaging of Spontaneous Canine Mammary Tumors using Fluorescent Contrast Agents. *Photochemistry and Photobiology, 70*, 87-94 (1999).
64. Hattery, D., Chernomordik, V., Loew, M., Gannot, I., Gandjbakhche, A. Analytical Solutions for Time-resolved Fluorescence Lifetime Imaging in a Turbid Medium Such as Tissue. *Journal of the Optical Society of America a-Optics Image Science and Vision 18*, 1523-1530 (2001).